# HIGH-POWER PROTON LINAC FOR APT; STATUS OF DESIGN AND DEVELOPMENT

G. P. Lawrence

Los Alamos National Laboratory, Los Alamos, NM, 87545, USA

## 1 INTRODUCTION AND OVERVIEW

In one of two options being considered for a new source of tritium, the US Department of Energy (DOE) is planning an Accelerator Production of Tritium (APT) plant [1] that would be built at its Savannah River Site in South Carolina. The facility will employ a high power linear accelerator to produce neutrons by spallation reactions of protons in tungsten and lead contained in a target/blanket (T/B) assembly. The fast neutrons produced in the target are moderated in the light water that cools the blanket elements, and then captured by $^3$He gas to produce tritium. The tritium is separated from the $^3$He by permeation through a palladium membrane, with cryogenic distillation used for isotopic purification.

The APT design is based on a 1700-MeV proton linac operated at 100 mA CW. However, changing tritium requirements may reduce the energy to 1030 MeV, so the plant has been designed in a modular

RFQ, the entire linac operates at a frequency of 700 MHz, with rf power supplied by 1-MW CW klystrons. After acceleration, a high-energy beam transport system (HEBT) consisting of magnetic focusing and bending elements conveys the beam to the T/B assembly. The architecture of the transport system depends on the machine energy, as indicated in Fig. 1. At the end of the HEBT, a raster beam expander transforms the beam into a rectangular, uniform large-area distribution, providing an acceptable power density in the target.

The linac design is driven strongly by the large amount of rf power required to accelerate the 100-mA CW beam. Efficient conversion is needed at each stage in the power train (from the ac grid to the beam) to minimize capital and operating costs. Other important design factors and considerations are the need to keep beam losses at a very low level, avoiding generation of beam halo, tight control of the high-power beam (in terms of the coupled beam/cavity/rf-drive interaction), current-
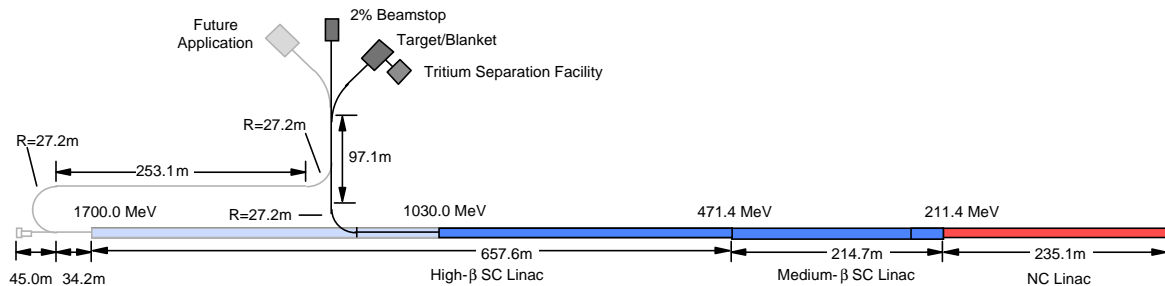


Fig.1 Modular design architecture for APT Plant.

configuration to provide construction flexibility. Figure 1 shows the architecture of the modular plant. Heavy shading and lines indicate the 1030-MeV configuration; light shading and dashed lines show the portions added in a 1700-MeV system.

The project Conceptual Design Report [2] was issued in April, 1997, and formal design of the plant technical and conventional systems has now begun. A program of engineering development and demonstration (ED&D) has been underway since 1995 to support the plant design and subsequent construction.

## 2 ACCELERATOR DESIGN

The APT linac is designed as a two-stage machine [3], using both normal-conducting (NC) and superconducting (SC) accelerating-cavity technologies. Except for the first accelerating structure, a 350-MHz

independent operation and tuning, and high operational availability. Parameter selection and cost/performance modeling to achieve these objectives have been discussed previously [4]; key parameters are listed in Table 1.

### 2.1 Normal-Conducting Low-Energy Linac

The low-energy NC linac accelerates a 100-mA proton beam to 211.4 MeV in copper water-cooled structures. A 75-keV injector using a microwave-driven ion source produces a continuous 110-mA proton beam. From this input, a 350-MHz, 8-m-long RFQ (radio-frequency quadrupole) produces a CW 100-mA beam at 6.7 MeV. This RFQ is built in four resonantly-coupled segments, with rf drive provided by three 1.2-MW CW klystrons through 12 windows; it provides a current independent match into the next accelerating section.

| Parameter | Normal-Conducting Linac | | | Superconducting Linac | | |
|---|---|---|---|---|---|---|
| | RFQ | CCDTL | CCL | $\beta = 0.64\text{-}1$ | $\beta = 0.64\text{-}2$ | $\beta = 0.82$ |
| Output energy (MeV) | 6.7 | 96.6 | 211.4 | 242.0 | 471.4 | 1700 (1030) |
| Struct. gradient $E_0T$ (MV/m) | 1.38 | 2.04-1.68 | 1.68-1.82 | 4.3-4.5 | 4.3-5.0 | 5.25 |
| Avg. gradient (MV/m) | 1.38 | 0.77-1.12 | 1.12-1.22 | 1.21-1.54 | 1.21-1.54 | 2.05 |
| Peak surface field (MV/m) | | | | 14.1-17.7 | 14.1-17.7 | 13.1-17.5 |
| Quadrupole lattice period (m) | | 8-9 $\beta\lambda$ | 9 $\beta\lambda$ | 4.877 | 6.181 | 8.540 |
| Section length (m) | 8.0 | 112.8 | 110.4 | 29.3 | 185.4 | 657.6 (298.9) |
| Phase-adv./period (deg) | – | 79-44 | 44-35 | 79-46 | 79-46 | 79-82 |
| No. of quadrupoles | – | 243 | 114 | 12 | 60 | 154 (70) |
| Quadrupole G•L prod. (T) | | 2.6-1.5 | 1.5-1.0 | 1.96 – 1.79 | 1.93 – 2.12 | 2.25 – 4.39 |
| Synchronous phase (deg) | - 90 to -33 | - 90 to -30 | -30 | - 30 to -35 | - 30 to -42 | -30 |
| Shunt impedance (MΩ/m) | – | 16-49 | 24-35 | | | |
| Copper rf losses (MW) | 1.26 | 5.0 | 6.8 | | | |
| Power to beam (MW) | 0.67 | 8.99 | 11.48 | 3.06 | 26.00 | 122.86 (55.86) |
| Power per klystron (MW) | 0.77 | 0.80-0.84 | 0.81-0.84 | 512-560 | 765-840 | 798-840 |
| Number of klystrons | 3 | 17+6 | 24+5 | 6 | 30 | 154 (70) |
| Trans. emitt. (mm-mrad)* | 0.16 | 0.17 | 0.17 | 0.16-0.19 | 0.16-0.19 | 0.19-0.17 |
| Long. emitt. (MeV-deg)* | 0.32 | 0.33 | 0.33 | 0.33-0.32 | 0.33-0.32 | 0.32-0.41 |
| Aperture radius (mm) | 2.3-3.4 | 10-17.4 | 17.4-31.9 | 65 | 65 | 80 |
| Aperture/beamsize ratio | – | 6.5-10 | 10-27 | 28-31 | 28-31 | 32-76 |

\* Normalized rms values, 700 MHz.  Quantities in parentheses are for a 1030-MeV output energy.

The RFQ is followed by $\pi/2$-mode coupled-cavity accelerating structures, each optimized for maximum rf-to-beam efficiency over a specific velocity range [5]. The first set of structures, which accelerates the beam to 96.6 MeV, is a 700-MHz CCDTL (coupled-cavity drift-tube linac) made up of 2-gap and 3-gap DTL cavities that are embedded in a FODO singlet focusing lattice. The latter begins with an 8-$\beta\lambda$ period and transitions to a 9-$\beta\lambda$ period at 10 MeV to provide additional space for quadrupoles and beam diagnostics. The quadrupoles are external to the cavity structures, separating the focusing and accelerating functions, and providing easy beam

energy and is free from phase-space transitions after the RFQ. Beam dynamics analyses and simulations show these factors to be important in terms of minimizing core emittance growth [6] and the generation of beam halo [7]. As seen in Table 1, both transverse and longitudinal emittance growth are negligible. To obtain a current-independent match between the NC linac and the SC linac (which has weaker focusing), the quadrupole strength is reduced gradually as the transition energy is approached.

The CCDTL and CCL are sectioned into rf super-modules, which are each powered by 4 to 7 klystrons. Each klystron distributes power to the accelerating struct-
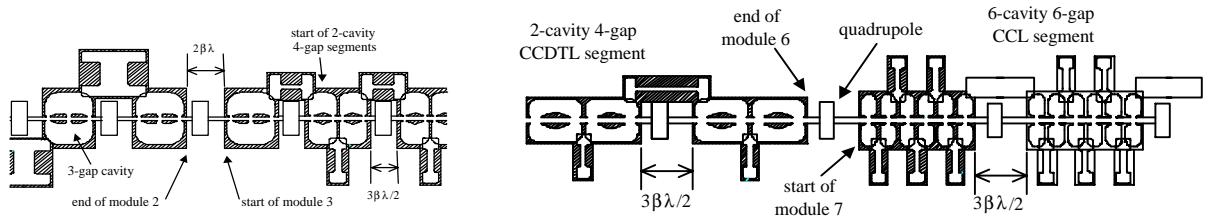


Fig. 2. CCDTL and CCL accelerating structure segments

alignment. Acceleration proceeds to 211.4 MeV in a 700-MHz side-coupled CCL that continues the 9-$\beta\lambda$ focusing period. Fig. 2 displays representative segments of the CCDTL and CCL.

The NC linac has a short focusing period that elongates with beta, and the average accelerating gradient is ramped up gradually from 0.77 to 1.2 MV/m. The result is a linac that has strong focusing at low beam

ure through four coaxial ceramic windows that are tested to 1-MW power levels [8]. The maximum rf power input to the cavities that is required from any of the klystrons is 0.84 MW, which allows for 10% control margin as well as rf transmission line losses. There are six supermodules in the CCDTL, with 28-57 segments per module. The CCL is divided into five supermodules, with 21-54 segments per module.

## 2.2 Superconducting High-Energy Linac

The SC high-energy linac consists of cryomodules containing two, three, or four 5-cell 700-MHz niobium SC accelerating cavities. Focusing is provided by NC quadrupoles in a doublet lattice located in the warm regions between cryomodules; these regions also contain the beam diagnostics. There are two kinds of SC cavity shapes, each type designed for efficient acceleration in a different velocity range. The cavity shape in the medium-beta section (211.4 MeV to 471.4 MeV) is optimized for $\beta = 0.64$, and in the high-beta section (471.4 MeV to 1700 MeV) for $\beta = 0.82$. The shapes are similar to the well-established elliptical designs for electron machines, but are compressed longitudinally in proportion to beta. Because the cavities are short and are driven independently, each section of the SC linac has a broad velocity bandwidth, which allows the gradient profile and output energy to be adjusted over a wide range. Because of the high beam current, the major design issue is not attainment of high cavity gradients, but high power rf coupler capability. Performance specifications of 140 kW and 210 kW have been chosen for the medium-$\beta$ and high-$\beta$ couplers respectively, values that are at the advancing edge of the demonstrated technology base. Each cavity is supplied by two antenna-type coaxial couplers mounted on opposite sides of the beam tube. Dual coaxial (warm) windows are planned, located so that they do not see the beam directly.

Figure 3 depicts the cryomodule, rf, and focusing-lattice architecture for the different sections of the SC linac. The high-$\beta$ section contains 77 (35) of the four-cavity cryomodules shown in the right-hand sketch. Two 1-MW 700-MHz klystrons are used to power pairs of looks structurally like one-half of the high-$\beta$ unit. Both are powered by a single 1-MW klystron. Earlier doublet-lattice medium-$\beta$ linac designs with 2-cavity cryomodules attempted a configuration in which a klystron powered cavities in adjacent cryomodules. In beam simulations that included machine errors, it was found that this architecture gave rise to significant emittance growth because of the large cavity-to-cavity phase/energy errors that were introduced.

Table 1 lists key parameters of the SC linac. The selection of cavity gradients and numbers of cells per cavity were restricted by the need to keep peak surface fields below a safe level and by the power-coupler specifications. The rf power distribution is governed by the need to fully utilize the 840-kW power available from each 1-MW klystron. The design specification for the average cavity $Q_0$ is taken as $5\times10^9$. A 2.15 K operating temperature for the niobium cavities has been selected to minimize the static and rf heat loads to the LHe refrigerator and cryo-distribution system. Total cryoplant loads are estimated at 14.5 kW at 2.15K and 22.4 kW at 45K, for a 1700-MeV linac. These loads will be handled by three identical LHe refrigerators that are about 50% larger than those in service at CEBAF.

## 2.3 Beam Dynamics

The key beam dynamics [9] goal is to achieve very low losses (< 0.1 nA/m at 1700 MeV) in order to assure unrestricted hands on maintenance for the linac. This is provided by strong focusing at low energies and avoidance of phase-space mismatches, coupled with apertures that are much larger than the rms beam size, with the largest aper-tures at high energies where the



Fig. 3. Medium-$\beta$ and high-$\beta$ cryomodule and rf architecture in superconducting linac.

adjacent cavities. The nominal energy gain per cavity is 4.0 MeV. The medium-$\beta$ SC linac is divided into two sections, both containing $\beta = 0.64$ cryomodules. The first section, starting at 211.4 MeV consists of six 2-cavity cromodules, and the second, starting at 242.0 MeV, consists of thirty 3-cavity cryomodules. Nominal energy gain per cavity is 2.6 MeV. The first section provides a transition between the short focusing period of the NC linac and the longer focusing period of the SC linac, and allows a current independent match to be obtained with minimal emittance growth.

The left-hand sketch in Fig. 3 shows the 3-cavity $\beta = 0.64$ cryomodules; the 2-cavity unit is not shown, but activation threat is greatest. In the NC linac, the aperture increases in steps to 64 mm, while in the SC linac it jumps to 130 mm at 211.4 MeV, and then to 160 mm at 471.4 MeV. Figure 4 shows 100,000-particle beam simulations for both an error-free machine design, and for one with a set of randomly chosen imperfections, with magnitudes about a factor of two worse than typical errors expected in operation. The simulations compare the linac aperture dimension with both the rms beam size and the radius of the outermost particle in the distribution (the halo). At full energy, the aperture ratio (ratio of aperture to rms-beam-size) is close to 80, providing a very large clearance for the beam halo. At low energies,
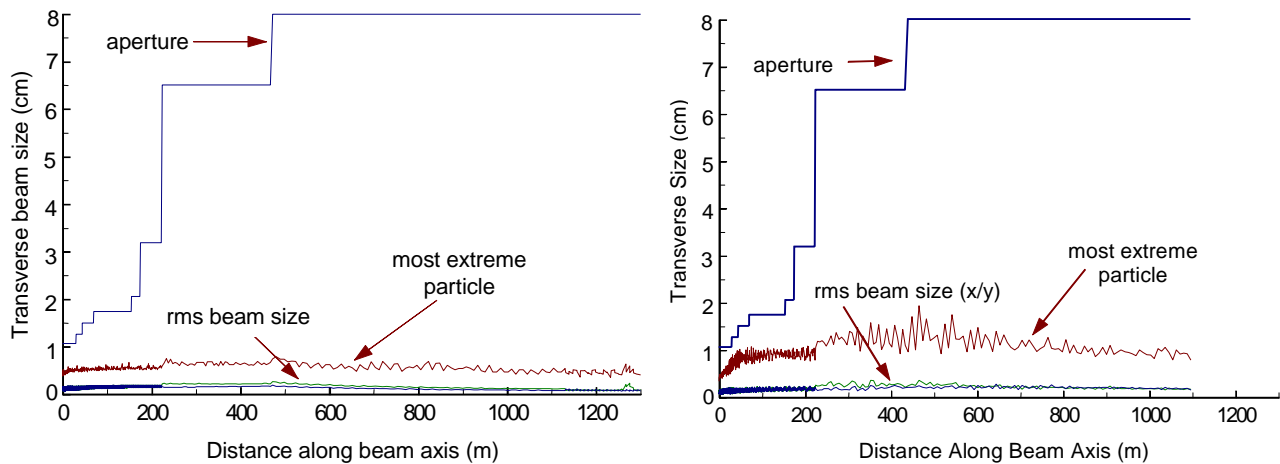
Fig. 4. Beam simulations for APT linac design showing rms beam size and radius of outermost particle, compared with aperture. Left: No machine errors. Right: Standard set of machine errors.

the clearance is less generous, and some small losses may occur.

## 2.4 Availability

Because the SC linac operates with short independently-driven accelerating cavities, the linac output energy may be adjusted over a wide range, providing considerable operational flexibility. Simulations confirm that, because of this feature, the SC linac is insensitive to a broad range of construction or operating errors and also can continue to function in a variety of off-normal conditions, such as having single klystrons, cavity pairs, and quadrupole pairs out of service. In order to meet the high annual availability goal for the accelerator (> 85%), redundancy schemes are used to provide excess rf drive in both the NC and SC linacs, but are implemented differently in each. The NC linac is divided into supermodules consisting of 100-150 coupled accelerating cells, with each unit supplied by n klystrons (typically 4 to 7), where only n-1 units are need-ed for operation. When an rf station fails, it is isolated by a waveguide switch and the accelerating structure drive iris is shorted. Power from the remaining klystrons is increased to compensate for the lost unit, and the supermodule continues to provide the full energy gain needed in that section. In the SC linac, redundancy is achieved by providing a modest level of reserve power in each rf station, above that needed to deliver the nominal output beam power, allowing increased energy gain in adjacent cryomodules to compensate for failed units. The power reserve is 5% in the high-β section and 9% in the medium-β section.

## 3 HIGH ENERGY BEAM TRANSPORT

A High Energy Beam Transport (HEBT) system [9] delivers the beam from the end of the linac to the (T/B). The HEBT focusing lattice continues the doublet-quadrupole optics in the high-β linac to a magnet switchyard.

Here the beam is directed either to a tuning beamstop that can take up to 2% of the full-energy beam power, or into the beam line serving the T/B assembly. This beam line terminates in a raster beam expander, which converts the small-diameter Gaussian-like beam distribution into a large-area rectangular (19 cm wide x 190 cm high) uniform distribution at the target. The beam expander consists of two sets of four sweep magnets driven with triangular waveforms by IGBT modulators at frequencies close to 500 Hz. One set is for the horizontal-plane sweep, and the other for the vertical plane. Because the sweep frequencies are slightly different, the raster system paints the T/B uniformly once per 30 ms. A multiply-redundant modulator fault detector system protects the T/B from excess beam power density due to degradation or interruption of the sweep pattern. In the modular plant configuration, the T/B is located near the end of the 1030-MeV linac, following a 10-period drift and a 90-degree bend. If the linac is built to 1700 MeV, the beam returns to this target line through a transport system consisting of a 180-degree bend, a straight beam channel parallel to the linac, and a reverse 90-degree bend. Beam dynamics studies have shown that the insertion of these bends, which are first-order achromats, have essentially no effect on beam loss and on the beam performance on the target. They do, however, introduce some additional operational complexity.

## 4 ENGINEERING DEVELOPMENT AND DEMONSTRATION (ED&D)

The APT accelerator design is supported by a broad ED&D program that will demonstrate and prototype key components and systems. The program (Fig. 5) consists of 1) a Low-Energy Demonstration Accelerator (LEDA) that will prototype the APT linac front end up to 20 MeV, 2) development of high-β and medium-β SC-cavity and cryomodule prototypes, and several smaller programs. LEDA [10] will consist ultimately of a proton injector, a

6.7-MeV 350-MHz RFQ, and a 20-MeV CCDTL section. Its purpose is to confirm beam performance parameters, demonstrate integrated operation at full CW power, assess overall availability, and identify component failure modes. The major stages involve 1) construction and testing of a 75-keV, 110-mA proton injector; 2) addition of a 350-MHz RFQ to accelerate a 100-mA CW proton beam to 6.7 MeV; and 3) addition of a 700-MHz CCDTL to accelerate the beam to 20 MeV.

The LEDA injector has been built and successfully tested at APT performance specifications (110 mA H+, <0.2 mm-mrad emittance). Construction and assembly of the RFQ is well advanced; the eight sections have been fabricated, and initial rf tuning of the whole structure is complete. The injector was recently successfully operated with a 1.25-MeV 267-MHz CW RFQ available from another program. Beam output current and transmission (100 mA, 85%) were as predicted, a strong validation of the codes used to design the APT RFQ.

A prototype of the highest-energy CCDTL segments (near 97 MeV) will be built and tested at full rf power to demonstrate RF coupling, manufacturability, and thermal performance of the section of the NC linac that is the most difficult to cool.
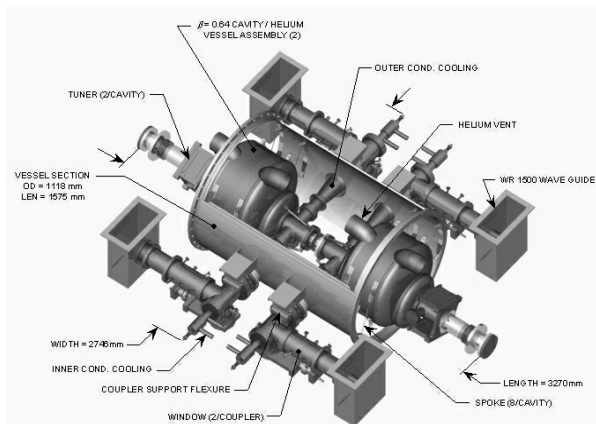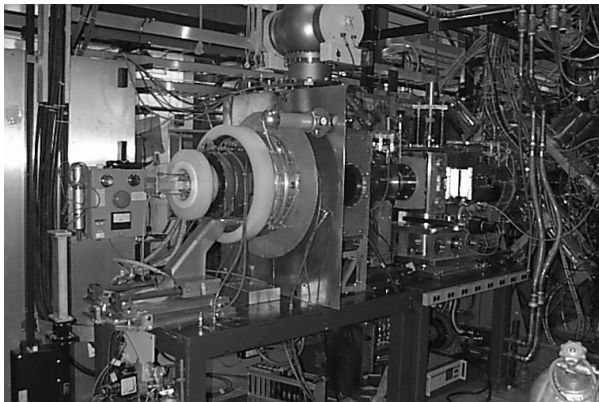




Fig. 5. ED&D program elements. Top: LEDA injector. Bottom: $\beta = 0.64$ 2-cavity cryomodule.

The SCRF ED&D program [11] has as its basis the $\beta = 1$ cryomodules operating successfully in several elec-

tron accelerators. For the APT SC linac, it is necessary to develop cryomodule prototypes containing the lower-$\beta$ cavity shapes needed for a proton accelerator. Development of these prototypes will confirm design parameters, component integration, and constructibility, and will support transfer of the technology to industry for manufacture of plant cyromodules. The elements of the SCRF program include: 1) fabrication and high-field testing of single-cell cavities; 2) evaluation of radiation damage to a prototype cavity; 3) fabrication and testing of high-power rf couplers; 4) fabrication and testing of multicell SC cavities; and 5) assembly and tests of complete prototype cryomodules. The first and second of these activities have already been successfully accomplished.

Other elements of the ED&D program include: 1) development of a prototype 1-MW 700-MHz High-Order-Mode Inductive-Output tube, which would offer improved efficiency and reliability (lower operating voltage) compared with a klystron, 2) construction and testing of a full scale raster beam expander prototype, 3) development and testing of high-power rf components (windows, waveguide valve, etc.), and 4) development of prototype diagnostics for measuring beam profiles at medium and high energies.

## 5 REFERENCES

[1] P.W. Lisowski, "The Accelerator Production of Tritium (APT) Project," Proc. 1997 Particle Accelerator Conf., Vancouver (May 1997).

[2] APT Conceptual Design Report, Los Alamos Report LA-UR-97-1329, April 15, 1997.

[3] G.P. Lawrence and T.P. Wangler, "Integrated Normal-Conducting/Superconducting High-Power Proton Linac for the APT Project," Proc. 1997 Particle Accelerator Conf., Vancouver (May 1997).

[4] G.P. Lawrence, et al., "Conventional and Superconduct-ing RF Linac Designs for the APT Project," Proc. 1996 Int. Linac Conf., Geneva, 710 (August 1996).

[5] J.H. Billen et al., "A Versatile High-Power Linac for Accelerator-Driven Transmutation Technologies, Proc. 1995 Particle Accelerator Conf., Dallas, IEEE No. 95CH35843, 1137 (1995).

[6] S. Nath, et al., "Beam Dynamics Design for the APT Integrated Linac," Proc. 1997 Particle Accelerator Conf., Vancouver (May 1997).

[7] T.P. Wangler, "New High Power Linacs and Beam Physics Issues," ibid.

[8] D. Rees, "Design of 250-MW CW RF System for APT," ibid.

[9] R.E. Shafer et al., "Overview of the APT High Energy Beam Transport and Beam Expanders," ibid.

[10] D. Schneider, "A Review of High Beam Current RFQ Accelerators and Funnels," Proc. 1998 European Particle Accelerator Conference, Stockholm (June, 1998).

[11] K.C.D. Chan et al., "Engineering Development of Super-conducting RF Linac for High-Power Applications," ibid.